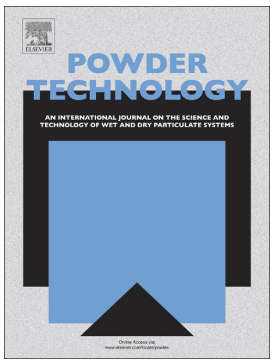

Numerical simulation of TiO2 nanoparticle synthesis by flame spray pyrolysis

Hosein Torabmostaedi, Tao Zhang

PII: S0032-5910(18)30057-3
DOI: https://doi.org/10.1016/j.powtec.2018.01.051
Reference: PTEC 13137

To appear in: *Powder Technology*

Received date: 17 September 2017
Revised date: 15 January 2018
Accepted date: 20 January 2018

Please cite this article as: Hosein Torabmostaedi, Tao Zhang , Numerical simulation of TiO2 nanoparticle synthesis by flame spray pyrolysis. The address for the corresponding author was captured as affiliation for all authors. Please check if appropriate. Ptec(2017), https://doi.org/10.1016/j.powtec.2018.01.051

Numerical Simulation of TiO2 Nanoparticle Synthesis by Flame Spray Pyrolysis

Hosein Torabmostaedi[1] and Tao Zhang[2]*

1. HSSMI Ltd. Birmingham, UK

2. Faculty of Science, Engineering and Computing, Kingston University, London, SW15 3DW, UK

* Corresponding author. Tel./fax:+44 208 4174103

E-mail address: T.Zhang@kingston.ac.uk

Abstract

A numerical method of combining CFD with the particle dynamics was developed to study the effect of processing parameters on the formation of TiO_2 nanoparticles by Flame Spray Pyrolysis. The computational model was validated by comparing with experimental measurements and used to predict the effects of production rates, type of dispersion gases and their flow rates. The results show that the predicted particle sizes and flame height are reasonably agree with experimental measurements therefore, it can be used to simulate the FSP process for the production of TiO_2. The simulation results show that when oxygen was used as dispersion gas, the spray flame height increases from 12 to 22.5 cm by increasing the TiO_2 production rate from 16 to 74 g h^{-1}. Similarly, when increasing the liquid feeding rate from 5 to 23.2 mL min^{-1} the flame height is increased from 12.5 to 24 cm using air as dispersion gas. Using air as dispersion gas results in slightly longer flames than that using oxygen. The primary particle diameter is equivalent or slightly smaller when using air instead of oxygen as dispersion gas.

Keywords: TiO_2 particles; FSP; Particle size control; Computational fluid-particle dynamics

1. Introduction

Nanostructured titanium dioxide (TiO_2) is considered to be one of the most popular photocatalysts for the photodegradation of organic pollutants due to its high photocatalytic activity, excellent stability for chemical and photocorrosions, commercial availability, and low price [1]. In 2010, the annual worldwide production of nanoscale TiO_2 was 10000 ton [2]. By 2015, the production is projected to increase to 201,500 tons [3]. The high surface area of nanoparticles is beneficial to many TiO_2-based devices, as it facilitates reaction/interaction between the devices and the interacting media, which mainly occurs on the surface or at the interface and strongly depends on the surface area of the material. Thus, the performance of TiO_2-based devices is largely influenced by the sizes of the TiO_2 building units, apparently at the nanometre scale [4]. Such properties have led to the development or use of TiO_2 nanoparticles for a wide variety of applications, including surface coatings, cosmetics, sensors and solar cells [5-7].

Different manufacturing processes have been used to produce nano sized TiO_2 particles. For example, Sun etc. synthesized spherical mesoporous titania particles by hydrolysis method using titanium tetrachloride under mild conditions [8]. Furlani etc. produced nano sized titania and titania–ceria powder mixtures using high energy ball milling [9]. Among the techniques used to produce nano particles, Flame Spray Pyrolysis (FSP) are one of the most promising processes in which the particle size can be fully controlled in narrow range. In FSP, the solution (liquid pre-cursor and fuel) is atomized by using an air-assisted nozzle to

form the droplets. The droplets are then evaporated and ignited by using a small pilot flame (i.e. positioned around the nozzle tip) to form solid nano particles.

To date the research on FSP made titania nanoparticles has progressed only in experimental fashion. Experiments were mostly focused on lab scale production while the higher scale requirements have never been investigated. Bickmore et al. investigated the production of FSP-made titania at production rates up to 25 g h^{-1} and compared the particle size and morphology with those produced in flame hydrolysis [10]. Although the size of product powders was similar ~ 35 nm, the FSP oxide powders were mostly spherical while those produced by flame hydrolysis had a blocky morphology and were necked, indicating that the powder remained in a hot environment long enough for sintering to commence. Their work showed that the FSP technique may be a useful alternative to flame hydrolysis for titania production.

Teoh et al. used FSP to produce TiO_2 nanoparticles with controlled specific surface area and crystallite size [11]. TiO_2 particles were synthesised at various production rates (9.6 to 22.5 g h^{-1}) by increasing the feed rate of the precursor solution (from 3 to 7 mL min^{-1}) while keeping the dispersion gas, supporting flame and sheath gas levels constant. They observed that the BET-equivalent average primary particle diameter was increased linearly from 11 to 21 nm with increasing precursor feed rate from 3 to 7 mL min^{-1}. This was expected since the combustion of the precursor mixture is an exothermic reaction, contributing to the overall increase in energy dissipation within the flame. Additionally, as the precursor feed flow rate increased, the particle concentration within the flame also increased. Higher particle concentration and flame heights favoured the coagulation and sintering of the particles and increased the particle size.

Schulz et al. investigated the effect of rapid quenching of FSP flames on the particle size and morphology of TiO_2. [12] They used the same burner geometry and operating parameters as the one used by Teoh et al. [11] however only one level of precursor feeding rate (5 mL min^{-1}) was used with small TiO_2 production rate of 16 g h^{-1}. Quench gas (oxygen) with a total flow rate of 40 L min^{-1} was injected radially into the spray flame. Using the rapid quenching, they could decrease the BET average diameter of TiO_2 nanopowders from 15.3 to 11 nm by decreasing the burner quench distance (BQD) from 12 to 4 cm above the burner.

Schimmoeller et al. [13] demonstrated the deposition of FSP-made airborne V_2O_5/TiO_2 nanoparticles directly onto mullite foam supports to create ready-to-use catalysts for the o-xylene conversion to phthalic anhydride. They scaled up the production rate of V_2O_5/TiO_2 nano powders by increasing the precursor concentration at a constant precursor feeding rate. It was observed that the particle size was increased from 17 to 29 nm when the production rate was increased from 17.2 to 87.2 g h^{-1}.

Several parameters need to be studied and optimized in order to have a controlled synthesis at high production rates. Since measuring the profile of the flame and the characteristics of the products during the process are expensive, time consuming and impossible for some parameters, numerical modelling was found to be an excellent tool for optimizing the FSP process.

In our previous studies [14,15], the computer simulations were carried out to optimize the nozzle geometries and processing parameters at medium and high production rate of zirconia nanoparticles in FSP. The results showed that it is possible to simulate the complete flame spray process without having to rely on experimental input data under certain conditions. In

this study, the efforts have been put through to improve the previous modelling by coupling the aerosol model with the gas dynamics in the CFD code through user-defined functions. This would reduce the time needed to import the gas dynamics data to the aerosol model for the calculation of the particle growth [14]. Furthermore, the effect of particle formation is accounted, hence, there won't be any need to set the initial conditions of the aerosol model based on the complete evaporation and decomposition of the precursor.

In this study, the framework of the previous [14,15] and current investigations described below were applied to high production of TiO_2 nanoparticles to understand the effects of processing parameters and to develop a technique to increase the process efficiency. However to use the current model for the optimization studies, validation with TiO_2 spray flames should be conducted to confirm that the gas and particle parameters are correctly accounted for.

To validate the current model, the model's predictions of flame temperature and particle size at different titania production rates were compared to those obtained by Schulz et al. and Teoh et al. for the lab scale production rate [11,12]. Then, the validated model was used for the process optimization of TiO_2 synthesis in FSP.

2. Model Development

2.1 Configuration of the Burner

Fig. 1a shows the schematic view of the FSP configuration which is consistent with the experimental setup of Schulz et al. and Teoh et al. [11,12]. A concentric two-phase nozzle

with a capillary of $d_o = 0.041\,\text{cm}$ in diameter and an annulus with gas size x (x is adjustable according to the pressure drop and mass flow rates, see Fig. 1a) was used for injecting the liquid solution and the atomization gas. The capillary was used to spray the solution of titanium iso-propoxide (TTIP, Aldrich, 97%; Buchs, Switzerland), diluted in a 11:5 (by volume) mixture of xylene (Fluka, 98.5%; Buchs, Switzerland) and acetonitrile (Fluka, 99.5%; Buchs, Switzerland) at constant 0.67 M concentration. Oxygen injected from the surrounding annulus was used as dispersion gas for both studies [11,12] at a flow rate of 5 L min^{-1} with a constant pressure drop of 1.5 bar across the nozzle tip. Premixed methane and oxygen were supplied through a circular slit (inner diameter 0.6 cm, slit width 0.001 cm, CH_4/O_2; 1.5 L min^{-1}: 3.2 L min^{-1}, respectively) to ignite the flame. Additional sheath O_2 (5 L min^{-1}) was supplied through a sintered metal plate ring (inner/outer diameter 1.8/3.4 cm).

A two-dimensional axisymmetric computational domain (height 40 cm, radius 5 cm, ~ 46000 cells, see Fig. 1b) was used to describe the spray flame. All the outlets including pilot flame, dispersion gas, sheath gas and the solvent/precursor mixture were included in the computation domain. Fine meshes were employed to the sensitive areas such as, the dispersion gas entrance and exit, and the centreline of the free-jet where high gradients are expected and great accuracy is required in order to capture the compressibility effects. A constant pressure condition was used at the outlets of the outside domain (1 atm). The appropriate under-relaxation factors were imposed to avoid instability in the solution.

2.2 Coupled CFD-monodisperse population balance (CFD-MPB) model

In FSP process, premixed fuel and precursor are atomized by using a gas-assisted nozzle to micron-sized droplets [16] which are subsequently evaporated in the flame. The formation

of particles begins when the precursor gas is going through a chemical reaction. In this method high temperature is needed to evaporate the precursor and provide the condition for the chemical reaction. In the process, the temperature of the flame varies from 2400 to 3300 K depending on the type of the oxidizer and the operation conditions. At the early stage, the partic1es are formed by gas-phase nucleation and grow by coagulation (particles collide with each other and stick to form agglomerates) and later they coalesce into larger particles. The shape of the final product is determined by the rates of coalescence and coagulation. If the rate of sintering is faster than that of the coagulation, the particles are spherical otherwise irregular agglomerate shape is developed [17].

In this study, the titanium (IV) isopropoxide was used as precursor material for the synthesis of TiO_2 particles. In the flame, evaporated TTIP molecules decompose thermally according to the following overall reaction. [18]

$$TTIP \rightarrow TiO_2 + 4C_3H_6 + 2H_2O$$

This reaction takes place even at temperatures as low as 250 ºC [19]. Propylene is one of the products after thermal decomposition of TTIP. If enough oxygen is supplied above the nozzle, the proplylene and the additional fuels used for the pilot flame and solvents (i.e. methane, xylene and acetonitrile) will decompose according to the following single step stoichiometric reactions:

$$C_3H_6 + 4.5O_2 \rightarrow 3CO_2 + 3H_2O$$

$$CH_4 + 2O_2 \rightarrow CO_2 + 2H_2O$$

$$C_2H_3N + 1.5O_2 \rightarrow CO_2 + H_2O + HCN$$

$$C_8H_{10} + 10.5O_2 \rightarrow 8CO_2 + 5H_2O$$

The monodisperse aerosol model proposed by Kruis et al. [17] used in our previous studies [14,15] was modified for the synthesis of TiO_2 nanoparticles in FSP. In the new model, the equations of total particle number concentration, surface area concentration and volume concentration undergo convection and diffusion in addition to being generated and depleted. This formulation is consistent with the monodisperse population balance models proposed in the literature previously for the flame synthesis of nanoparticles. [20,21]

The rate of change of particle number concentration, N, is given by

$$\frac{\partial}{\partial z_i}\left(\rho u_i N - \Gamma_k \frac{\partial N}{\partial z_i}\right) = I - \frac{1}{2}\beta(\rho N)^2 \quad (1)$$

The first two left-hand side terms in Eq. (1) describe the convection and diffusion of the particles in turbulent flow. The particle formation rate, I, is calculated based on the mass flux imbalance in each grid cell [21]. Where ρ is the density of TiO_2 and z is the distance above nozzle exit.

$$I = \frac{-N_A}{V_{cell} M_T} \sum_{i=1}^{n} m_i X_{T,i} \quad (2)$$

where N_A is the Avogadro number, V_{cell} is the cell volume, M_T is the molecular weight of TTIP, n is the number of cell faces, m_i is the signed (positive for out- and negative for in-

flow) mass flux through cell face i, and $X_{T,i}$ is the mass fraction of the precursor at cell face i.

The Fuchs interpolation function for Brownian coagulation in the free molecule and continiuum [17, 22]; was used to calculate the collision kernel for irregular shaped aggregates

$$\beta = 8\pi D r_c \left[\frac{r_c}{2r_c + \sqrt{2}g} + \frac{\sqrt{2}D}{c r_c} \right]^{-1} \tag{3}$$

where the particle diffusion coefficient D ($m^2\ s^{-1}$), transition parameter g (m) and particle velocity c ($m\ s^{-1}$) are needed to calculate the coagulation kernel, are given by following expressions [17]:

$$D = \frac{k_b T}{6\pi c r_c} \left[\frac{5 + 4kn + 6kn^2 + 18kn^3}{5 - kn + (8+\pi)kn^2} \right] \quad \text{with} \quad kn = \frac{\lambda}{r_c} \tag{4}$$

$$c = \sqrt{\left(\frac{8k_b T}{\pi \rho\ v} \right)} \tag{5}$$

$$g = \frac{1}{(6 r_c l)} \left[(2r_c + l)^3 - \left(4r_c^2 + l^2\right)^{1.5} \right] - 2r_c \quad \text{with} \quad l = \frac{8D}{\pi c} \tag{6}$$

where λ is the gas mean free path, k_b is Bolzmann's constant.

The sintering effect on the agglomerate surface area was given by Koch and Friedlander [23]:

$$\frac{\partial}{\partial z_i}\left(\rho c A - \Gamma_k \frac{\partial A}{\partial z_i}\right) = I a_0 - \frac{\rho\left(A - N a_s\right)}{t_{\sin}} \tag{7}$$

where A is the total agglomerate area concentration (m^2/kg_{gas}), and a_0 and a_s are the surface area of TiO_2 monomer, $t_{\sin}$ is the sintering time and surface area of a completely fused (spherical) aggregate respectively [17],

$$a_0 = \frac{6v_0}{d_{monomer}} \quad \text{with} \quad v_0 = \frac{M_{TiO_2}}{\rho} \times N_A \quad \text{with} \quad d_{monomer} = \left(\frac{6v_0}{\pi}\right)^{1/3} \tag{8}$$

and

$$a_s = \left(\frac{V}{v_0}\right)^{2/3} a_0 \tag{9}$$

where v_0 and $d_{monomer}$ are the volume and diameter of the TiO_2 monomer, respectively. The total agglomerate volume concentration, V, is given by Kruis et al., [17]

$$\frac{\partial}{\partial z_i}\left(\rho u_i V - \Gamma_k \frac{\partial V}{\partial z_i}\right) = I v_0 \tag{10}$$

The characteristic sintering time, t_{sin}, is the time needed for the sinter neck diameter to reach 83 % of the initial primary particle diameter (given by Kobata et al., [24]). Here the performance of the following $t_{\sin}$ has been investigated

$$t_{\sin} = 7.4.10^{16} \times d_p^4 \times T \exp\left(\frac{258000}{RT}\right) \quad (11)$$

$$t_{\sin} = 9.7 \times 10^{15} \times d_p^4 \times T \exp\left(\frac{258000}{RT}\right) \quad (12)$$

$$t_{\sin} = k_0 \times d_p^4 \frac{T}{1400} \exp\left(\frac{148000}{R}\left(\frac{1}{T} - \frac{1}{1400}\right)\right) \quad (13)$$

where k_0 is the pre-exponential term, d_p is the primary particle diameter (m) and T is the temperature (K). Eq. (11) is derived by Kobata et al. (1991) [24] when they studied the sintering rate of TiO_2 for temperatures between 1123 K and 1473 K. Using this equation, [24] predicted a final primary particle size of 50 nm which was in a reasonable agreement with experimental data. Seto et al. [25] proposed the Eq. (12) and simulated the evolution of the particle size which was in good agreement with the measured TiO_2 primary particle diameters (d_p=10–100 nm) for temperatures between 300 K and 1673 K. Johannessen et al. [26] proposed effective sintering time of ultrafine titania particles (Eq. 13) by comparing their model with experiments for TiO_2 production via oxidation of $TiC1_4$ vapor for temperatures up to 2000 K. The difference between the models assumed to be due to different reactors and different procedure for obtaining the t_{sin} . In the first two models, the furnace reactors with temperatures below 1700 K was used whereas in the third model the diffusion flame with temperatures up to 2000 K was used.

The model-predicted titania particle sizes calculated useing three proposed sintering time provided by Kobata Seto and Johannessen et al. [24-26] were given in Fig. 3 and compared with the particles found by experiments (given by Schulz and Teoh et al.. The characteristic

coalescence time given by Johannessen et al. [26] with $k_0 = 1 \times 10^{30}$ was chosen here (See Fig. 3)

2.3 Numerical implementation

Eqs. (1)-(13) along with the governing equations for the conservation of mass, momentum, energy, turbulence, chemical species, droplet species and radiation (explained fully in previous paper [14]) form the complete set of equations of the CFD–MPB model and were solved using the FLUENT pressure-based 2D axisymmetric solver and Green-Gauss Node based gradient option. The MPB equations were written in C++ language and the code was coupled with the main flame dynamics module of the CFD solver as user-defined function. A second-order upwind discretization scheme was used since it ensured the accuracy, stability and convergence. SIMPLEC algorithm (SIMPLE-Consistent) described by Van Doormaal and Raithby [27] was used for pressure-velocity coupling, which uses a relationship between velocity and pressure corrections to enforce mass conservation and to obtain the pressure field. Turbulence was described with the Shear Stress Transport (SST) $k-\omega$ [28]. For the thermodynamic database, eleven species were included (TTIP, TiO_2, O_2, C_3H_6, H_2O, CH_4, CO_2, C_2H_3N, HCN, C_8H_{10}, and N_2).

3. Results and discussion

3.1 Model validation

In this study, the flame temperature profiles and the final primary particle size were used for model tuning and validation. The flame temperatures obtained in the axial direction at different height above the burner were measured by Schulz et al. [12] using non-intrusive

Fourier transform infrared (FTIR) emission/transmission (E/T) spectroscopy technique [29]. Two pairs of identical paraboloidal mirrors guide the IR beam through the flame and a 0.4 cm iris at the first focal point defines the beam diameter in the flame centre (second focal point). The particles were collected by a vacuum pump on a glass microfiber filter. The final primary particle size was calculated based on the measured specific surface area (SSA) of the TiO_2 powder by N_2 adsorption at 77 K using the Brunauer–Emmett–Teller (BET) equation theory [11,12] . More details of the experimental apparatus and procedures can be found in the cited references.

The computational model was tested with the experimental data reported by Schulz and Teoh et al. [11,12] for the synthesis of TiO_2 nanoparticles using TTIP as the precursor. To validate the predicted temperature profile of titania flame during FSP, the measurement reported by Schulz et al. was used. [12] The precursor solution was fed through the central capillary of the nozzle at a feeding rate of 5 mL min^{-1}, resulting in TiO_2 production rate of 16 g h^{-1}.

Fig. 2 shows the comparison of calculated and measured [12] temperature profiles along the burner axis (centreline). CFD-average prediction for IR beam with 0.4 cm diameter going through the flame at different height above burner is also included to be consistent with measurements (Schulz et al., [12]) Close to the nozzle exit, the predicted centerline temperature is lower than the average value which shows that the maximum temperature is slightly off centre due to the evaporation of droplets. This behaviour was also observed by Schulz et al. [12] for the low heights above the burner. The measured flame temperature increases rapidly to ~2500 K at 5 cm above the burner and begins to decrease to ~1000 K at 12 cm above the burner. The simulated maximal flame temperature was ~600 K higher than

the measured data, assumed to be attributed to low signal intensity in the optically thick part of the flame. In addition, Schulz et al. [12] has not performed the tomographic construction on FTIR measured profile which would cause under prediction for the measured temperatures (Kammler et al., [30])

To validate the predicted final particle diameter of titania in FSP, the measurements of Schulz et al. and Teoh et al. [11,12] were used. Fig. 3 shows the predicted final titania diameters along the centreline for different precursor feed rates (3-7 mL min^{-1} - production rate of 9.6-22.5 g h^{-1}) along with the measured data (open symbols). Three sintering time equations (Kobata et al., [24]); incorporated in the particle dynamics model and the results were compared with the measured data (Schulz and Teoh et al. [11,12]). As it can be seen in Fig. 3, the model of Johannessen et al. [26] is in a very good agreement with the measured particle diameter at all production rates while the results were under predicted by 54 and 58 % for the sintering models of Seto and Kobata et al. [24, 25] respectively.

3.2 Effect of production rate using different oxidant/dispersion gas

Using the numerical models developed in this study, the spray flame structure and ultimately product diameters were simulated at low titania production rates. The simulation results showed that the numerical models are in reasonable agreement with on-line characterizations at different production rates, thus, they can be used for equipment design and process optimization in FSP. The following processing parameters were studied for the production of TiO_2 nanoparticles: at different poduction rates using oxygen or air as oxidant/dispersion gases.

In our previous study [14], it was shown that at medium production rate ($\leq$ 300 g h^{-1} ZrO_2) and using low precursor concentration, the primary particle size could be closely controlled by keeping the gas to liquid flow ratio (GLFR) and dispersion gas pressure drop at constant values of 1300 and 7 bar, respectively. In this study, the framework of our previous investigation [14] was examined for the flame spray synthesis of titania by titanium isopropoxide (TTIP) decomposition.

Fig. 4 shows spray flames of 0.67 M TTIP in xylene/acetonitrile solutions producing titania at 16, 50, and 74 g h^{-1} (corresponds to precursor feeding rates of 5, 15.6, and 23.2 mL min^{-1}) using oxygen (a-c) or air (d-f) as dispersion gas at constant GLFR and pressure drop of 1300 (corresponds to dispersion gas feeding rates of 6.5, 20.3, and 30.2 L min^{-1}) and 7 bar, respectively.

Tamaekong and Liewhiran et al. [31,32] adapted the operating parameters of Schulz et al. [12] and investigated the production of zinc and tin dioxide nanoparticles by diluting the 0.5 M zinc naphtenate (Aldrich, 8 wt% Zn) and tin (II) 2-ethylhexanoate (Aldrich, 95%) in xylene (Carlo Erba, 98.5%), respectively. In both FSP productions, the flame height was observed to be within 10-12 cm. They also observed an increasing rate for flame height at higher precursor concentrations. Comparing this height range (10-12 cm) with the flame temperature measurement of Schulz et al. [12], the temperature range of 1000-1200 K was obtained. In this study, the lower limit of the temperature (1000 K) was chosen to indicate the flame height due to higher precursor concentration in this study (0.67 M TTIP).

When oxygen was used as dispersion gas, the spray flame height increases from 12 to 22.5 cm by increasing the TiO_2 production rate from 16 to 74 g h^{-1} (Fig. 4a-c). The increase of the

liquid feeding rate from 5 mL min^{-1} (corresponding to 16 g h^{-1} TiO_2) to 23.2 mL min^{-1} (74 g h^{-1}) increases the supplied fuel energy from 9.36 to 43 MJ h^{-1}. This prolongs the time for fuel combustion and results in longer flames. Similarly, when increasing the liquid feeding rate from 5 to 23.2 mL min^{-1} the flame height is increased from 12.5 to 24 cm using air as dispersion gas (Fig. 4d-e). Using air as dispersion gas results in slightly longer flames than that using oxygen since carbonaceous components burn slower resulting in lower temperatures.

The slower burning rate of carbonaceous components can be clearly seen in Fig. 5a which shows the conversion of TTIP (solid lines) and xylene (dashed lines) along the burner axis for the spray flame producing 74 g h^{-1} TiO_2 using oxygen (black lines) and air (blue lines). The conversion of TTIP is completed rather fast, approximately within 1.2 and 3 cm from the burner tip when using oxygen and air as dispersion gas, respectively. It should be noted that Fig. 5a reports the conversion of TTIP as dictated by thermal decomposition (hydrolysis) as an overall reaction. [33] This was explained fully in section 2.2. The complete conversion of xylene is delayed by 4 cm when using air as dispersion/oxidant gas. This is attributed from the lower oxygen availability above the nozzle exit (Fig. 5b) which decreases the intensity of fuel/oxidant mixing and slows down the xylene oxidation rate.

The TTIP decomposition reaction is strongly related to the temperature distribution. The lower temperatures of spray flames when using air as dispersion gas can be seen in Fig. 6 which shows the predicted temperature along the burner axis (centreline) of the flames shown in Fig. 4. Using air as dispersion gas, the maximum temperature in higher production rates (corresponds to 50 and 74 g h^{-1}) reduced by ~20% while at lower production rate (16 g h^{-1}) this decrease was only 9 %. The high temperature of the flame at low production rate is

mostly due to the heat contribution from supporting methane/oxygen flame. Similar behaviour was also seen by Mädler et al. [34] when they studied the temperature structure during synthesis of silica nanoparticles in FSP. At higher production rates the heat contribution from the supporting methane/oxygen flame decreases as more dispersion gas has to be heated up.

Fig. 7 shows the evolution of the total agglomerate number concentration, N, for spray flame producing 74 g h^{-1} TiO_2 with oxygen (solid line) or air (dashed line) as dispersion gas using the temperature history described in Fig. 6.

Fig. 8 shows the predicted diameter of the TiO_2 primary particles as a function of production rate at a constant GLFR and pressure drop of 1300 and 7 bar using air and O_2 as dispersion gases at 0.67 M TTIP in xylene/acetonitrile. As the solution feeding rate is increased from 5 to 23.2 mL min^{-1} (corresponding to TiO_2 production rates of 16-74 g h^{-1}), the particle diameter increases from 14 to 17.8 nm using oxygen as dispersion gas. Although the GLFR and pressure drop were kept constant in this study, the diameter of TiO_2 nanoparticles has increased with an increment of 1.4 nm at each 25 g h^{-1} increment. The results in this section show that the behaviour of TiO_2 growth in spray flames is different from that of zirconia studied in the previous investigation [14].

The primary particle diameter is equivalent or slightly smaller when using air instead of oxygen as dispersion gas. The prediction of similar particle diameters for both air and oxygen as dispersion gas is in agreement with FSP studies at medium production rates of SiO_2 (Mueller et al., [34]) but is in disagreement to that of zirconia (Torabmostaedi et al., 2013). The results in our previous study (Torabmostaedi et al., [14]) showed that replacing oxygen

with air as dispersion gas was able to reduce the particle size by 25 %. Mueller et al. [34] observed that the average primary particle diameter was similar for GLMR above 1.2 at a silica production rate of 200-300 g h^{-1}. In this study the GLFR kept constant at 1300 which corresponds to GLMR of ~2.

Conclusions

A computation model was developed to understand the effects of processing parameters and to develop a technique to increase the process efficiency for the production of TiO_2 nanoparticles at higher production rate up to 74 g h^{-1}. The model was validated by comparing with experimental results published in literatures. The validated model was used to predict the effects of processing parameters, types of atomization gases and production rates. The results show that the predicted particle sizes and flame height are reasonably agree with experimental measurements therefore, it can be used to simulate the FSP process for the production of TiO_2. The simulation results show that when oxygen was used as dispersion gas, the spray flame height increases from 12 to 22.5 cm by increasing the TiO_2 production rate from 16 to 74 g h^{-1}. Similarly, when increasing the liquid feeding rate from 5 to 23.2 mL min^{-1} the flame height is increased from 12.5 to 24 cm using air as dispersion gas. Using air as dispersion gas results in slightly longer flames than that using oxygen. The primary particle diameter is equivalent or slightly smaller when using air instead of oxygen as dispersion gas.

Acknowledgements

The research leading to these results has received funding from the European Community's Seventh Framework Programme (FP7/2007-2013) under grant agreement no. 228885.

References

1. Jang, H. D., Kim, S-K. (2001). Controlled synthesis of titanium dioxide nanoparticles in a modified diffusion flame reactor. Materials Research Bulletin, 36, 627-637.
2. Piccinno, F., Gottschalk, F., Seeger, S., Nowack, B. (2012). Industrial production quantities and uses of ten engineered nanomaterials in Europe and the world. Journal of Nanoparticle Research, 14, 1109.
3. Research and Markets Report. (2011). The World Market for Nanoparticle Titanium Dioxide (TiO_2). 68 pages. http://www.researchandmarkets.com/research/4beff0/
4. Chen, X, Mao, S. S. (2006). Titanium Dioxide Nanomaterials: Synthesis, Properties, Modifications, and Applications. Chemical Reviews, 107, 2891-2959.
5. Quagliarini, E., Bondioli, F., Goffredo, G. B., Cordoni, C., Munafò, P. (2012). Self-cleaning and de-polluting stone surfaces: TiO_2 nanoparticles for limestone. Construction and Building Materials, 37, 51-57.
6. Baraton, M-I., Merhari, L. (2004). Surface chemistry of TiO_2 nanoparticles: influence on electrical and gas sensing properties. Journal of the European Ceramic Society, 24, 1399-1404.
7. Tan, B., Wu, Y. (2006). Dye-sensitized solar cells based on anatase TiO_2 nanoparticle/nanowire composites. The Journal of Physical Chemistry, 110, 15932-15938.
8. Sun, A., Li, Z., Li, M. Xu, G., Cui, P., Room temperature synthesis of spherical mesoporous titania, (2010), Powder Technology, 201, 130-137.
9. Furlani, E., Aneggi, E., leonora Leitenburg, C., Maschio, S. , (2014), High energy ball milling of titania and titania–ceria powder mixtures, Powder Technology, 254, 591-596
10. Bickmore, C. R., Waldner, K. F., Baranwal, R., Hinklin, T. Treadwell, D. R., Laine, R. M. (1998). Ultrafine titania by flame spray pyrolysis of a titanatrane complex. Journal of the European Ceramic Society, 18, 287-297.
11. Teoh, W. Y., Mädler, L., Beydoun, D., Pratsinis, S. E., Amal, R. (2005). Direct (one-step) synthesis of TiO_2 and Pt/TiO_2 nanoparticles for photocatalytic mineralisation of sucrose. Chemical Engineering Science, 60, 5852-5861.

12. Schulz, H., Mädler, L., Srobel, R., Jossen, R., Pratsinis, S. E., Johannessen, T. (2005). Independent control of metal cluster and ceramic particle characteristics during one-step synthesis of Pt/TiO_2. Journal of Materials Research, 20, 2568-2577.

13. Schimmoeller, B., Schulz, H., Pratsinis,, S. E., Bareiss, A., Reitzmann, A., Kraushaar-Czarnetzki, B. (2006). Ceramic foams directly-coated with flame-made V_2O_5/TiO_2 for synthesis of phthalic anhydride. Journal of Catalysis, 243, 82-92.

14. Torabmostaedi, H., Zhang, T., Foot, P., Dembele, S., Fernandez, C. (2013). Process control for the synthesis of ZrO_2 nanoparticles using FSP at high production rate. Powder Technology, 246, 419-433.

15. Hosein Torabmostaedi, Tao Zhang, Effect of nozzle geometry and processing parameters on the formation of nanoparticles using FSP, Chemical Engineering Research and Design, 92 (2014) 2470-2478.

16. Heine, M. C., Mädler, L., Jossen, R., Pratsinis, S. E. (2006). Direct measurement of entrainment during nanoparticle synthesis in spray flames. Combustion and Flame, 144(4), 809-820.

17. Kruis, F. E., Kusters, K. A., Pratsinis, S. E., Scarlett, B. (1993). A simple model for the evolution of the characteristics of aggregate particles undergoing coagulation and sintering. Aerosol Science and Technology, 19(4), 514-526.

18. Okuyama, K., Ushio, R., Kousaka, Y., Flagan, R. C., Seinfeld, J. H. (1990). Particle generation in a chemical vapor deposition process with seed particles. AIChE Journal 36 (3), 409–419.

19. Chen, P.-L., Chen, I.W. (1993). Reactive cerium (iv) oxide powders by the homogeneous precipitation method. Journal of the American Ceramic Society, 76 (6), 1577–1583.

20. Schild, A., Gutsch, A., Muehlenweg, H., Pratsinis, S. E. (1999). Simulation of Nanoparticle Production in Premixed Aerosol Flow Reactors by Interfacing Fluid Mechanics and Particle Dynamics. Journal of Nanoparticle Research, 1 (2), 305-315.

21. Gröhn, A-J., Buesser, B., Jokiniemi, J-K., Pratsinis, S. E. (2011). Design of Turbulent Flame Aerosol Reactors by Mixing-Limited Fluid Dynamics. Industrial & Engineering Chemistry Research. 50 (6), 3159–3168

22. Seinfeld, J. H. (1986). Atmospheric Chemistry and Physics of Air Pollution. New York: John Wiley & Sons.

23. Koch, W., Friedlander, S. K. (1990). The effect of particle coalescence on the surface area of a coagulating aerosol. Journal of Colloid and Interface Science, 140(2), 419-427.

24. Kobata, A., Kusakabe, K., Morooka, S. (1991). Growth and transformation of TiO_2 crystallites in aerosol reactor. AIChE Journal, 37(3), 347–359.

25. Seto, T., Hirota, A., Fujimoto, T., Shimada, M., Okuyama, K. (1997). Sintering of polydisperse nanometer-sized agglomerates. Aerosol Science and Technology, 27(3), 422-438.

26. Johannessen, T., Pratsinis, S. E., Livbjerg, H. (2001). Computational analysis of coagulation and coalescence in the flame synthesis of titania particles. Powder Technology, 118(3), 242–250.

27. Van Doormaal, J. P., Raithby, G. D. (1984). Enhancements of the simple method for predicting incompressible fluid flows. Numerical Heat Transfer, 7(2), 147-163.

28. Menter, F. R. (1994). Two-equation eddy-viscosity turbulence models for engineering applications. AIAA-Journal, 32(8), 1598-1605.

29. Best, P. E., Carangelo, R. M., Markham, J. R., Solomon, P. R. (1986). Extension of emission-transmission technique to particulate samples using FT-IR. Combustion and Flame, 66(1), 47-66.

30. Kammler, H. K., Pratsinis, S. E., Morrison, P. W., Hemmerling, B. (2002). Flame temperature measurements during electrically assisted aerosol synthesis of nanoparticles. Combustion and Flame, 128(4), 369-381.

31. Tamaekong, N., Liewhiran, C., Wisitsoraat, A., Phanichphant, S. (2009). Sensing characteristics of flame-spray-made Pt/ZnO thick films as H_2 gas sensor. Sensors, 9, 6652-6669.

32. Liewhiran, C., Tamaekong, N., Wisitsoraat, A., Phanichphant, S. (2009). H_2 sensing response of flame-spray-made Ru/SnO_2 thick films fabricated from spin-coated nanoparticles. Sensors, 9, 8996-9010.

33. Mädler, L., Pratsinis, S. E. (2002). Bismuth Oxide Nanoparticles by Flame Spray Pyrolysis. Journal of the American Ceramic Society, 85(7), 1713-1718.

34. Mueller, R., Mädler, L., Pratsinis, S. E. (2003). Nanoparticle synthesis at high production rates by flame spray pyrolysis. Chemical Engineering Science, 58(10), 1969–1976.

Figures

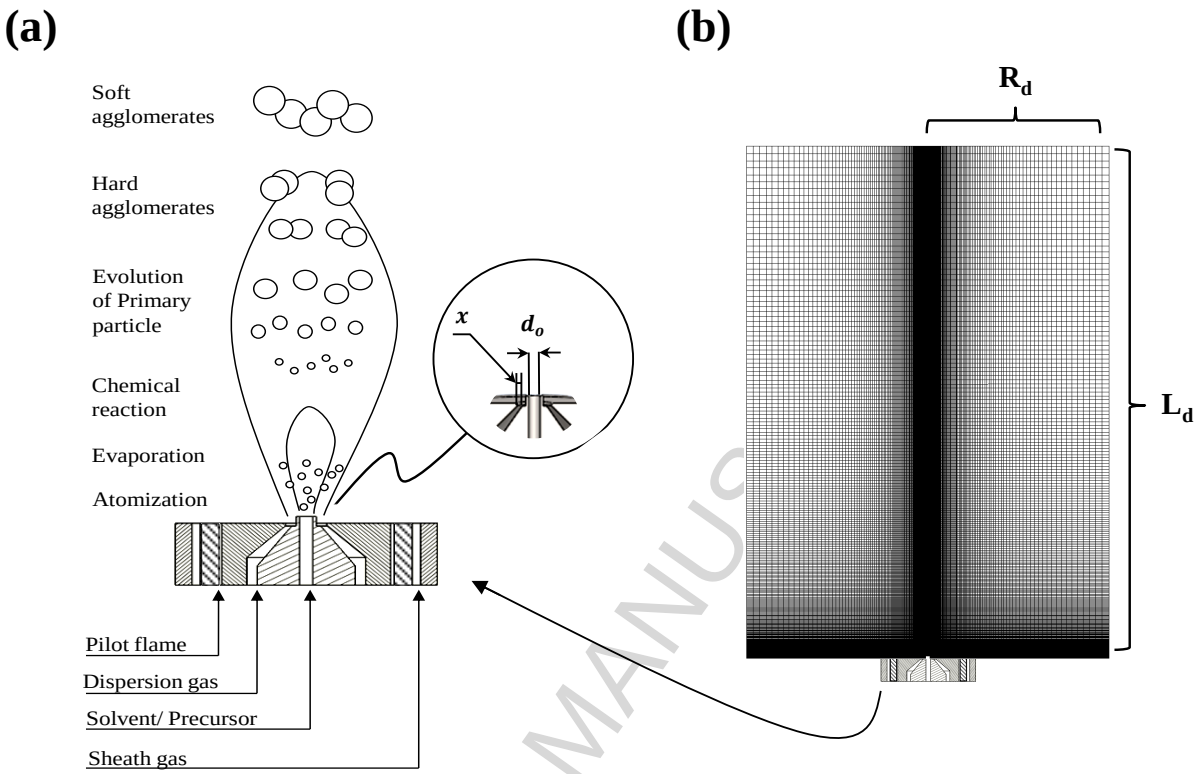

Fig. 1. Schematic of the (a) FSP configuration and (b) computational mesh. Legend for inputs to the computational mesh: x is the gap size of the annulus for the dispersion gas/oxidant, d_0 is the internal diameter of the nozzle orifice size, and R_d and L_d are the radius and length of the computational domain (i.e. outlets), respectively.

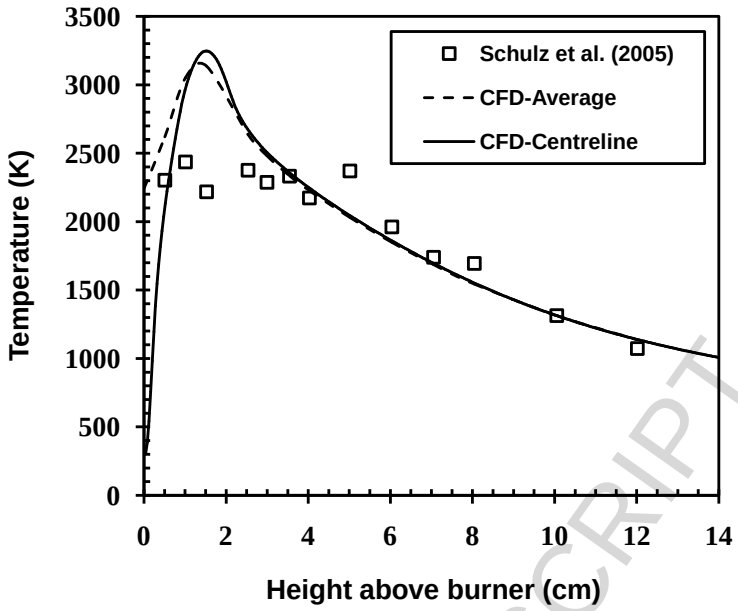

Fig. 2. The comparison of the calculated and measured flame temperature profiles of TiO_2 spray flames along the centreline for TiO_2 production rate of 16 g h^{-1}.

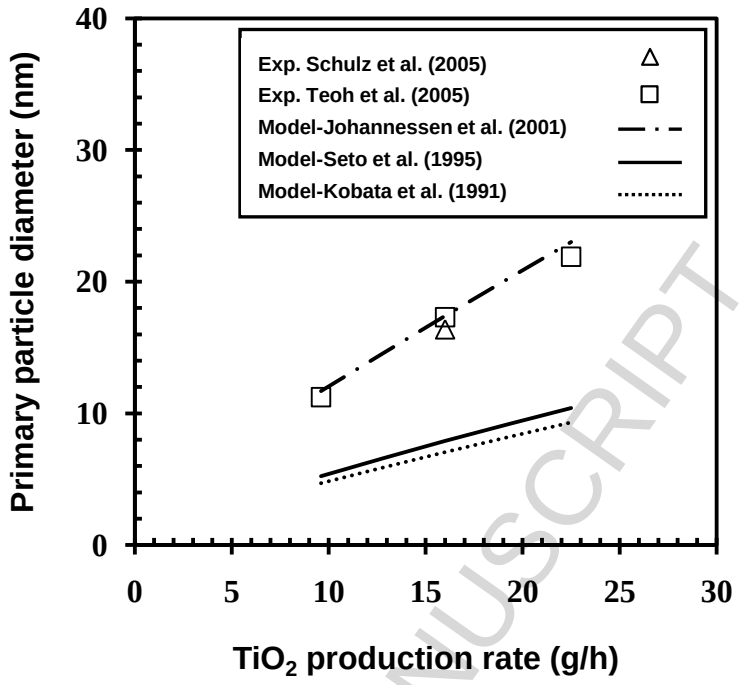

Fig. 3. Comparison between calculated and measured (Schulz et al., 2005; Teoh et al., 2005) final particle size as a function of TiO_2 precursor solution feed rate at 0.67 M TTIP concentration in xylene/acetonitrile using three different models for the prediction of characteristic sintering time.

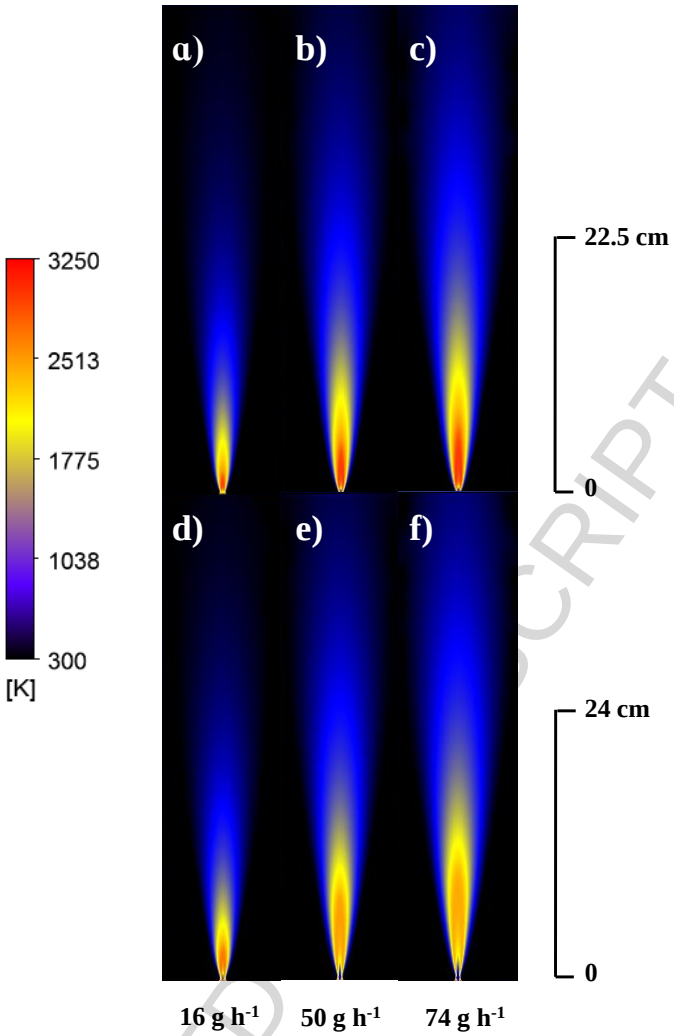

Fig. 4. Spray flames (0.67 M TTIP in xylene/acetonitrile) producing 16, 50 and 74 g h^{-1} of TiO_2 using oxygen (a-c) or air (d-f) as dispersion gas with an additional 5 L min^{-1} of sheath oxygen and constant GLFR and dispersion gas pressure drop of 1300 and 7 bar, respectively.

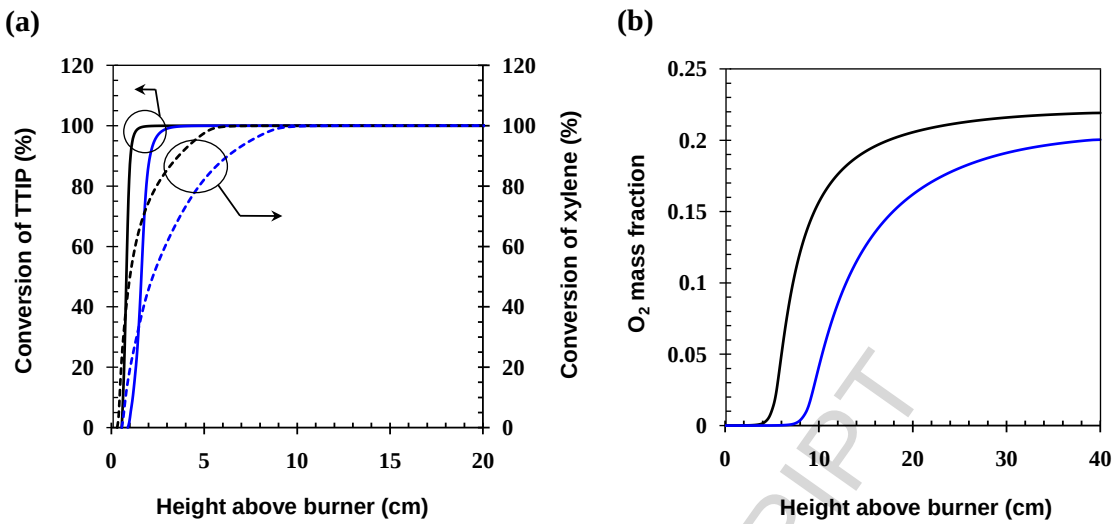

Fig. 5. Predicted (a) conversion of TTIP (solid lines) and xylene (dashed lines) and (b) oxidant mass fraction of FSP flame producing 74 g h^{-1} of TiO_2 along the burner axis (centreline) as a function of height above burner (HAB) using oxygen (black lines) and air (blue lines) as oxidant/dispersion gas.

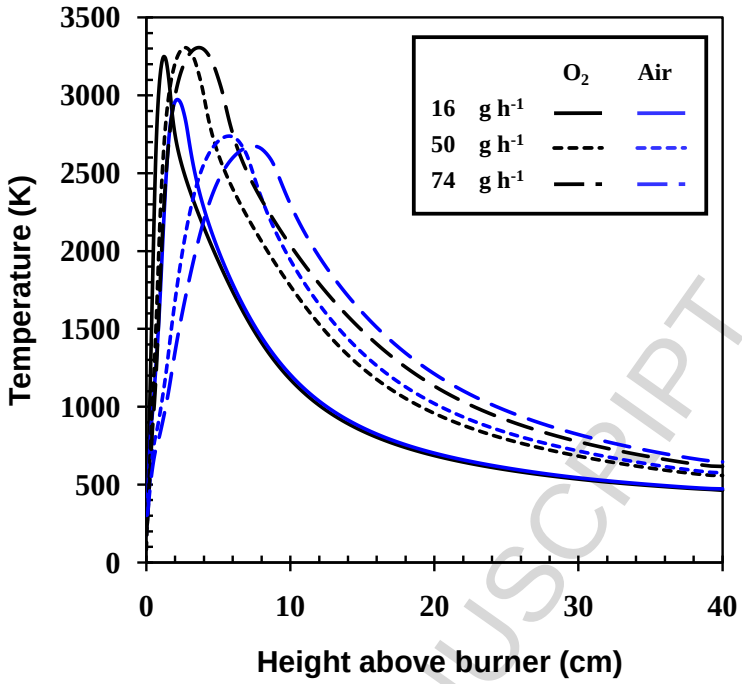

Fig. 6. Predicted flame temperature along the burner axis (centreline) of FSP flames as a function of HAB for various production rates using oxygen (blue lines) and air (black lines) as dispersion gas.

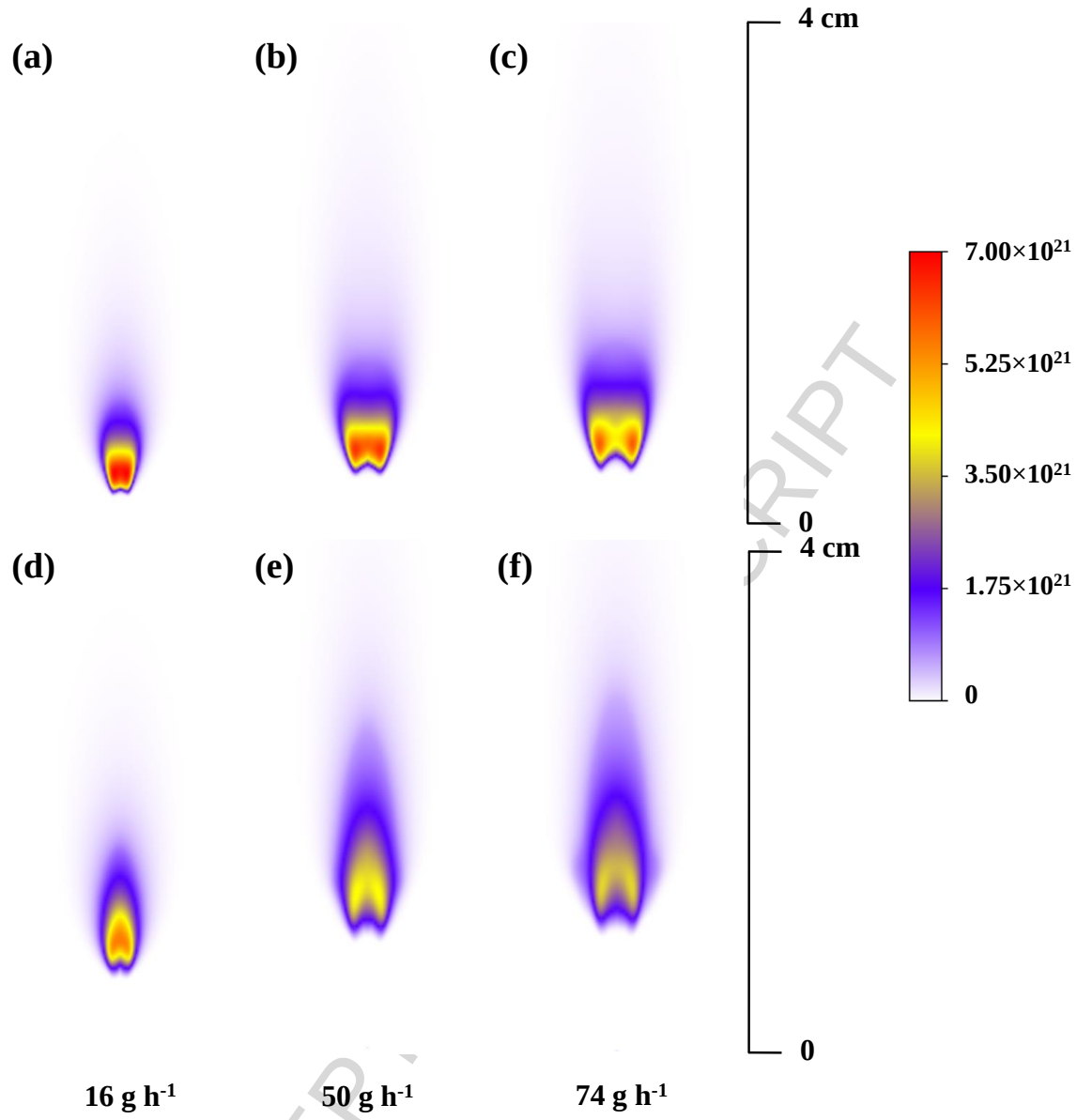

Fig. 7. Predicted total agglomerate number concentration above the burner for various TiO_2 production rates using oxygen (a-c) and air (d-f) as dispersion gas.

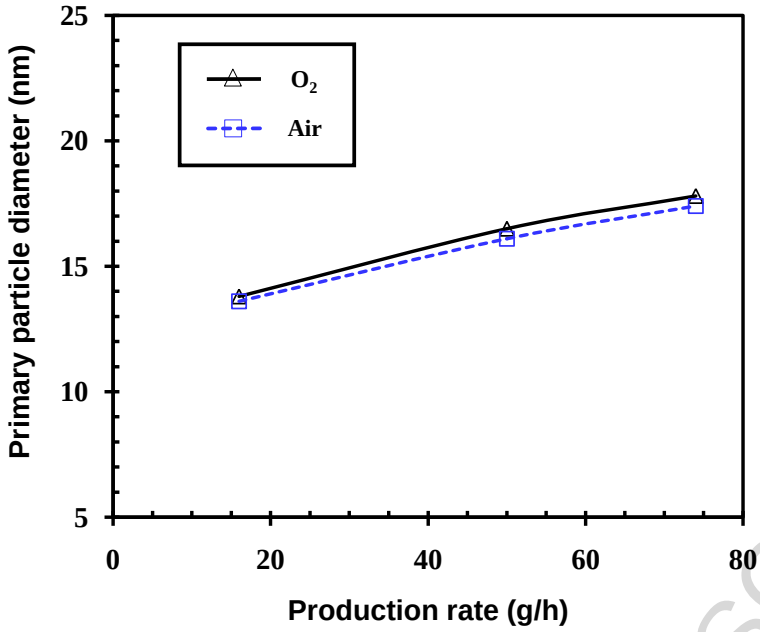

Fig. 8. Predicted primary particle diameter as a function of TiO_2 production rate using oxygen or air as dispersion gas.

Graphical abstract

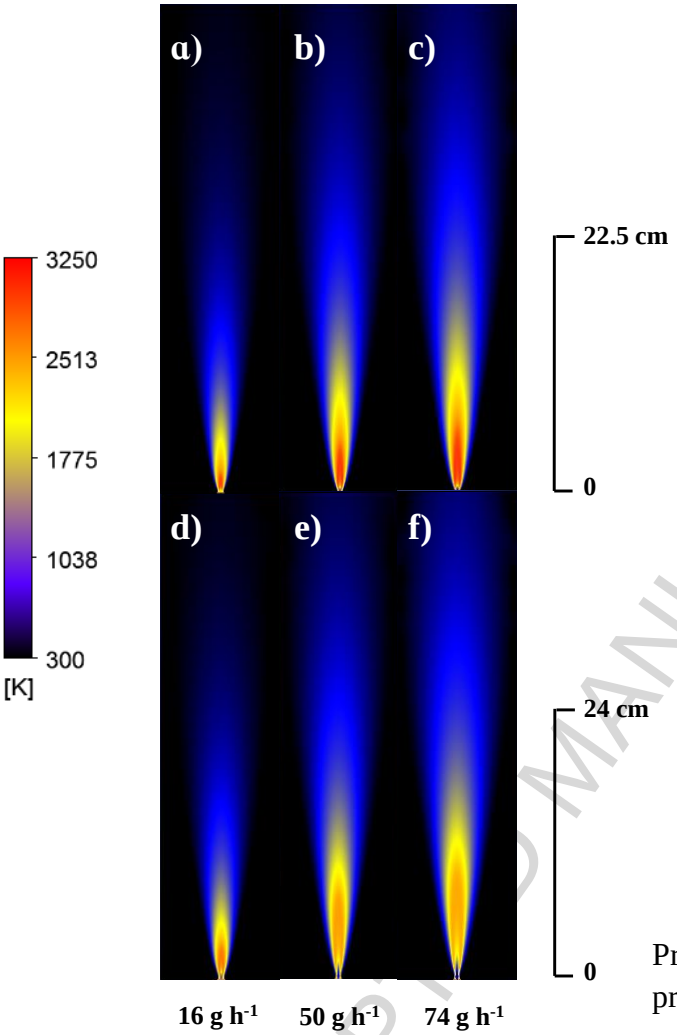

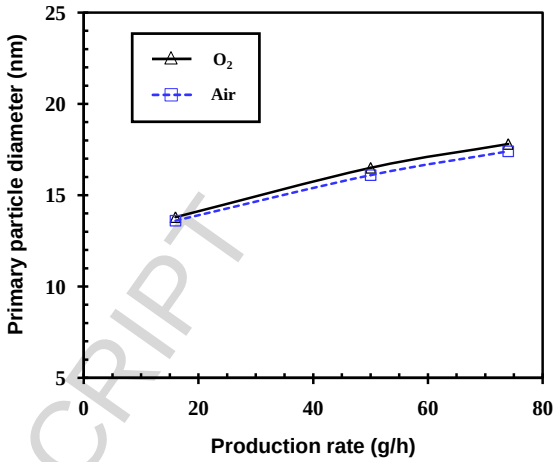

Predicted primary particle diameter as a function of production rate using different atomization gases.

Predicted spray flames at different production rate

Highlights:

The research cover:

1) Developed a CFD model to simulate the growth of TiO_2 nanoparticles in FSP.
2) The employed mathematical models were validated against experiments.
3) Predict the effect of processing parameters on flame structure.
4) Predict the effect of processing parameters on the final particle size.
5) Provide methodology for particle size control.